Ultrasonics Sonochemistry 77 (2021) 105681

Contents lists available at ScienceDirect

Ultrasonics Sonochemistry

journal homepage: www.elsevier.com/locate/ultson

Effect of ultrasonication time on microstructure, thermal conductivity, and viscosity of ionanofluids with originally ultra-long multi-walled carbon nanotubes

Bertrand Jóźwiak [a,*], Heather F. Greer [b], Grzegorz Dzido [c], Anna Kolanowska [a], Rafał Jędrysiak [a], Justyna Dziadosz [d], Marzena Dzida [d,*], Sławomir Boncel [a,*]

[a] Silesian University of Technology, Department of Organic Chemistry, Bioorganic, Chemistry and Biotechnology, Bolesława Krzywoustego 4, 44-100 Gliwice, Poland
[b] University of Cambridge, Department of Chemistry, Cambridge CB2 1EW, UK
[c] Silesian University of Technology, Department of Chemical Engineering and Process Design, Marcina Strzody 7, 44-100 Gliwice, Poland
[d] University of Silesia in Katowice, Institute of Chemistry, Szkolna 9, 40-006 Katowice, Poland

ARTICLE INFO

Keywords:
Ultrasonication time
Ionanofluids
Microstructure
Thermal conductivity
Viscosity

ABSTRACT

The stability along with thermal and rheological characteristics of ionanofluids (INFs) profoundly depend on the protocol of preparation. Therefore, in this work, the effect of ultrasonication time on microstructure, thermal conductivity, and viscosity of INFs containing 0.2 wt% of originally ultra-long multi-walled carbon nanotubes (MWCNTs) and four different ILs, namely 1-propyl-1-methylpyrrolidinium bis(trifluoromethylsulfonyl)imide, 1-butyl-1-methylpyrrolidinium bis(trifluoromethylsulfonyl)imide, 1-ethyl-3-methylimidazolium thiocyanate, or 1-ethyl-3-methylimidazolium tricyanomethanide, was studied. The INFs were obtained by a two-step method using an ultrasonic probe. The ultrasonication process was performed for 1, 3, 10, or 30 min at a constant nominal power value of 200 W. The obtained results showed that for the shortest sonication time, the highest thermal conductivity enhancement of 12% was obtained. The extended sonication time from 1 to 30 min caused the cutting of MWCNTs and breaking the nanoparticle clusters, leading to a decrease in the average length of the nanotube bundles by approx. 70%. This resulted in a decline in thermal conductivity even by 7.2% and small deviations from the Newtonian behavior of INFs.

1. Introduction

Ionanofluids (INFs) are a modern class of dispersions that consist of nanometer-sized solid particles (metals, oxides, carbon nanoparticles, etc.) dispersed in ionic liquids (ILs). INFs combine the advantages of ILs and nanofluids. They are characterized by higher thermal conductivity than pure ILs, as well as non-flammability and enhanced thermal stability than conventional nanofluids. Such an augmentation causes that INFs have great potential as heat transfer fluids, heat storage fluids, anti-wear lubricants, solar absorbing paints, and many others [1–6]. Among the variety of nanoparticles, there are carbon nanotubes (CNTs), particularly their multi-wall structural variant, which constitute the most promising high aspect ratio (quasi-one-dimensional) INF component [7]. This fact derives from their unique characteristics of physico-chemical performance 'enchanted' in the individual forms. The application of long MWCNTs in INFs was recently justified also by the economy [8].

One of the key elements influencing the long-term stability, thermophysical properties (specific heat capacity, thermal conductivity, convective heat transfer coefficient, pressure loss), and rheological characteristics of INFs is the uniform distribution of nanoparticles as they tend to agglomerate and sediment because of high surface energy [9]. There are two possible procedures for obtaining stable INFs: (i) single-step (bottom-up) approach and (ii) two-step (top-down) approach. In the single-step method nanoparticles are synthesized directly in ILs, while in the two-step method nanoparticles are first produced as dry powders by chemical/physical techniques and then dispersed in ILs via intensive ultrasonic treatment, high-shear mixing, ball milling, etc. [10]. Nonetheless, on a large scale, only a two-step approach is economically justified as the production of nanopowders has reached the industrial level [11].

The most common method of dispersing nanoparticles in ILs is the

* Corresponding authors.
E-mail addresses: bertrand.jozwiak@polsl.pl (B. Jóźwiak), marzena.dzida@us.edu.pl (M. Dzida), slawomir.boncel@polsl.pl (S. Boncel).

https://doi.org/10.1016/j.ultsonch.2021.105681
Received 28 June 2021; Received in revised form 19 July 2021; Accepted 19 July 2021
Available online 25 July 2021

ultrasonic treatment with probe or bath sonicators. The process is based on the propagation of high amplitude ultrasonic pressure waves of frequencies from 20 kHz to 1 MHz [12]. The energy transferred into ILs leads to the rapid formation, growth, and collapse of microcavities (microbubbles) which can locally increase pressure and temperature up to hundreds of atmospheres and thousands of Kelvins, respectively, and generate extreme shear forces and sonochemical effects [13]. All those effects cause breaking and dispersing of nanoparticle clusters as well as mixing and homogenization of INFs. Ultrasonic treatment is faster, more effective, and more resistant to contamination than conventional methods for mixing and dispersing nanoparticles in a liquid medium. However, it has some flaws, especially when using a probe sonicator [6]. For example, in the case of carbon nanotubes (CNTs), the concentrated high-energy pressure waves and long exposure times may cause various structural and topological defects in the sp^2-hybridized C—C only-carbon network. This can result in a high amorphous sp^3-carbon content, augmented exfoliation, nanotube unzipping toward graphenoids [14–17], and length reduction of CNTs, all of which have a significant impact on the thermophysical properties of obtained nanodispersions [12,18,19].

There is little literature on the influence of ultrasound treatment conditions on the microstructure as well as thermal and rheological properties of INFs. Most of the research in the field was carried out under constant sonication settings [20–31]. The notable exceptions were works of Wittmar et al. [32,33], who investigated rheological properties of INFs containing 0.5 wt% 95% anatase TiO_2 with average particle size 5 nm or 100% anatase TiO_2 with average particle size from 5 to 26.4 nm and 1-ethyl-3-methylimidazolium bis(trifluoromethylsulfonyl)imide [Emim][NTf_2], 1-ethyl-3-methylimidazolium tetrafluoroborate [Emim][BF_4], 1-butyl-3-methylimidazolium tetrafluoroborate [Bmim][BF_4], or 1-hexyl-3-methylimidazolium tetrafluoroborate [Hmim][BF_4], prepared with various sonication times up to 4 h. They concluded that the rheological behavior of nanodispersions was complex and depended on the type of IL. Sonication up to 2 h did not affect the rheology of INFs containing hydrophobic [Emim][NTf_2], whereas longer ultrasonic treatment resulted in the loss of Newtonian character of the nanodispersions in the case of 100% anatase TiO_2. On the other hand, the rheological properties of INFs based on hydrophilic ILs did not depend on the sonication time. Another work was carried out by França et al. [34], who investigated stability of INFs composed of 0.5 or 1 wt% MWCNTs (Baytubes C150 HP with mean outer diameter 13–16 nm and length 1–10 μm) dispersed in trihexyltetradecylphosphonium dicyanamide [$P_{6,6,6,14}$][$N(CN)_2$], trihexyltetradecylphosphonium bromide [$P_{6,6,6,14}$][Br], 1-ethyl-3-methylimidazolium thiocyanate [Emim][SCN], 1-butyl-3-methylimidazolium thiocyanate [Bmim][SCN], 1-ethyl-3-methylimidazolium tricyanomethanide [Emim][$C(CN)_3$], or 1-butyl-3-methylimidazolium tricyanomethanide [Bmim][$C(CN)_3$]. They noted that an extension of the sonication time (up to 1.5 h) did not improve the stability of INFs.

Much more widely explored in the area of ultrasound treatment duration were the conventional nanofluids (NFs). For instance, Wang et al. [35,36] applied various sonication times (3–120 min) when preparing nanodispersions containing graphite flakes (0.03–1 vol%) and distilled water, ethylene glycol, or poly-alpha-olefin. They found that shorter sonication time favored the formation of highly viscous NFs, especially at high nanoparticle loadings, while longer ultrasound treatment decreased both the viscosity and thermal conductivity.

It seemed that the high power of sonication could break large graphite agglomerates into small pieces (with average flake diameter of 7.3, 4.1, and 1.9 μm after 20, 60, and 120 min sonication, respectively, based on the statistics from SEM images), increasing thermal contact resistance. On the other hand, Amrollahi et al. [37], who investigated dispersions containing ethylene glycol and 0.5, 1.0, 2.0, or 2.5 vol% single-wall carbon nanotubes (SWCNTs), reported that for higher sonication time (1–24 h) the nanoparticle clusters became looser, and thermal conductivity began to rise. This was most likely related to the increased nanoparticle-fluid interface. Different observations were made by Asadi et al. [38], who analyzed the behavior of NFs containing distilled water and MWCNTs (0.1, 0.3, or 0.5 vol%), prepared at various ultrasound treatment duration (10–80 min). They found that increasing sonication time led to a gentle enhancement in thermal conductivity which reached its maximum at ca. 60 min, and then began to drop. The optimal sonication conditions could be related to more homogenous dispersion and minimum nanoparticle agglomeration. Likewise, prolonged ultrasound treatment might lead to a shortening of MWCNTs length and reduction of their interactions as well. Hence, the optimization might mean reaching a compromise between the deagglomeration of originally long nanotubes and their cutting at the level of individual nanotubes. Such a phenomenon was observed by Yu et al. [39], who examined the influence of sonication time (30–120 min) on the quality of NF containing 0.025 wt/vol% SWCNTs in an aqueous solution of 1 wt/vol% sodium deoxycholate as the stabilizing surfactant.

As the literature review shows [40], the microstructure and thermophysical properties of NFs and INFs are indeed very complex issues. Our research group is doing intensive scientific work to untie this Gordian knot. Recently, we studied the thermophysical properties of low-viscosity INFs consisting of 1-ethyl-3-methylimidazolium thiocyanate [Emim][SCN] and MWCNTs (in-house grown via chemical vapor deposition, CVD) with high aspect ratios of 6300 and 11000. We discovered an extraordinary improvement of thermal conductivity up to 43.9% for 1 wt% MWCNTs [41]. For the first time, we determined the thickness of the interfacial nanolayer (ca. 4 nm), which played a key role in enhancing the thermal properties of INFs. Furthermore, we investigated the actual heat transfer performance of INFs containing 0.1–0.25 wt% originally 440 μm-long MWCNTs and [Emim][SCN] in laminar flow regime, taking into account both gains (improved convective heat transfer coefficient) and losses (increased pressure drop) during the flow of INFs in horizontal cylindrical tube [8]. The new proposed figures of merit, performance evaluation criterion (PEC) and efficiency-price index (EPI), clearly indicated that the use of INFs for heat transfer purposes is justified from both engineering and economic points-of-view.

Now, this work aims to study the effect of ultrasonication time on microstructure, thermal conductivity, and rheological properties of INFs originally containing 770 μm ultra-long MWCNTs dispersed in ILs characterized by low viscosity and relatively high thermal conductivity, namely 1-ethyl-3-methylimidazolium thiocyanate [Emim][SCN] and 1-ethyl-3-methylimidazolium tricyanomethanide [Emim][$C(CN)_3$] [42], as well as moderate viscosity and rather low thermal conductivity, namely 1-propyl-1-methylpyrrolidinium bis(trifluoromethylsulfonyl) imide [Pmpyr][NTf_2] and 1-butyl-1-methylpyrrolidinium bis(trifluoromethylsulfonyl)imide [Bmpyr][NTf_2] [42].

2. Materials and methods

2.1. Materials

In our study, the INFs were prepared via a two-step procedure: (i) synthesis of nanomaterial in the form of dry powder and (ii) direct dispersion of the nanomaterial into a base IL using a high-power ultrasound dispersing device.

The dispersed phase of INFs consisted of originally ultra-long 'in-house 16h' MWCNTs (aspect ratio 11,000) synthesized in our laboratory via 16 h c-CVD, according to the previously reported methodology [43].

Table 1
Characteristics of ultra-long 'in-house 16h' MWCNTs used in this study.

Average length (μm)	Average diameter (nm)	Aspect ratio (–)	Specific surface area ($m^2 \cdot g^{-1}$)	Density ($g \cdot cm^{-3}$)	Carbon purity (%)
770	60–80	11,000	22	2.1	98

The detailed specification of the 'in-house 16h' MWCNTs sample can be found in Table 1. The morphology of obtained MWCNTs is shown in Fig. 1 in the form of SEM and TEM micrographs acquired using microscopes TESCAN MIRA3 FEG SEM at 5 kV and Thermo Scientific (FEI) Talos F200X G2 TEM at 200 kV, respectively. At lower magnification (Fig. 1A,B), originally ultra-long 'in-house 16h' MWCNTs display a fibrous bundle morphology, while TEM analysis revealed increasing graphitization of walls (i.e., high sp^2-carbon atoms content) when moving from the outer less-developed walls (richer in sp^3-carbon atoms) (Fig. 1C,D).

The continuous phase of studied INFs consisted of four commercial ILs obtained from IoLiTec, Germany: hydrophobic 1-propyl-1-methylpyrrolidinium bis(trifluoromethylsulfonyl) imide [Pmpyr][NTf_2] and 1-butyl-1-methylpyrrolidinium bis(trifluoromethylsulfonyl)imide [Bmpyr][NTf_2], as well as hydrophilic 1-ethyl-3-methylimidazolium thiocyanate [Emim][SCN], and 1-ethyl-3-methylimidazolium tricyanomethanide [Emim][$C(CN)_3$]. The ILs were first dried and degassed under argon at 2 mbar (Heidolph rotary evaporator combined with the SC 920 G vacuum pump system) at 105 °C for 6 h, and then the water content was determined via the Karl Fischer method by TitroLine 7500 (SI Analytics, Germany). Table 2 summarizes the specification of ILs.

2.2. Sample preparation

The 20 mL samples of INFs were prepared by dispersing 0.2 wt% of 'in-house 16h' MWCNTs in base ILs using probe sonicator UP200St (Hielscher Ultrasonics GmbH, Germany) with preset nominal values of power (200 W), frequency (26 kHz), and amplitude (100%). The appropriate mass of the nanoparticles was determined via analytical balance ACN220G (Axis, Poland) of $\pm 1 \cdot 10^{-4}$ g precision. Raw MWCNT-IL suspensions were subjected to ultrasound treatment for 1, 3, 10, or 30 min. The energies supplied to each sample during the sonication were equal to 0.060, 0.18, 0.60, or 1.8 Wh·mL^{-1}, respectively. Each sample was placed in a water-jacketed beaker which ensured adequate cooling (temperature below 50 °C). Prepared INFs containing pyrrolidinium-based ILs [Pmpyr][NTf_2] and [Bmpyr][NTf_2] proved to be stable for more than six months while nanodispersions with imidazolium-based ILs [Emim][SCN] and [Emim][$C(CN)_3$] sedimented after approx. two days, regardless of sonication time.

2.3. Microstructure analysis

Observations of the morphological structure of INFs were carried out via the conventional bright-field method using an optical microscope CH30 (Olympus, Japan) equipped with MPlan N 50×/0.75 objective and 5.1 MP camera ODC 832 (Kern, Germany). The statistical analysis of the length of MWCNT bundles for each sample, based on 150 measurements conducted in the ImageJ® software, enabled the determination of five statistical parameters: minimum value, maximum value, arithmetic mean, standard deviation, and polydispersity index.

2.4. Thermal conductivity measurement

The hot-wire technique was applied for thermal conductivity measurements of INFs at 25 °C. The thermal conductivity was measured using KD2 Pro Thermal Properties Analyzer (Decagon Devices Inc., USA) with a single needle KS-1 sensor of 1.3 mm diameter and 60 mm length. The appropriate temperature of a sample was ensured by Open Bath Circulator ED-5 (Julabo GmbH, Germany) with ethylene glycol. The temperature was gradually checked by the thermal sensor built into the KD2 Pro with a precision of 0.01 °C. After obtaining thermal equilibrium (ca. 30 min), three readings of KD2 Pro were recorded at 15 min intervals and averaged. The uncertainty of measurements was ±5%. The correctness of KD2 Pro measurements was verified by a supplied verification standard of glycerin. More details can be found in our previous work [41].

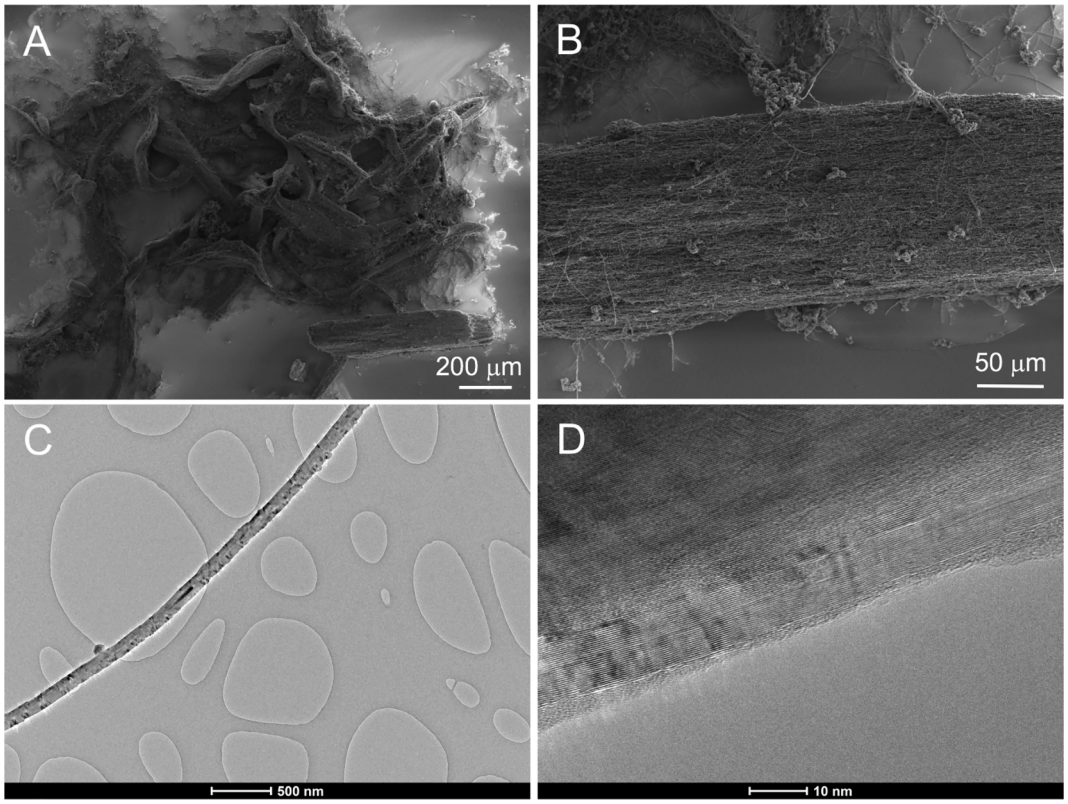

Fig. 1. SEM images of low (A) and higher magnification (B), and TEM images (C, D) of the herein used, as-grown originally ultra-long, i.e., 770 µm 'in-house 16h' MWCNT(s); darker spots in (C) correspond to mainly endohedral residues of Fe-based phases from the CVD synthesis.

Table 2
Specification of the commercial ILs used in this study.

Name	Acronym	CAS number	Mass fraction purity[a]	Water content (ppm)	Halides
1-propyl-1-methylpyrrolidinium bis(trifluoromethylsulfonyl)imide	[Pmpyr][NTf_2]	223437–05-6	>0.99	<100[a]/16[b]	<100 ppm[a]
1-butyl-1-methylpyrrolidinium bis(trifluoromethylsulfonyl)imide	[Bmpyr][NTf_2]	223437-11-4	>0.99	<100[a]/24[b]	<100 ppm[a]
1-ethyl-3-methylimidazolium thiocyanate	[Emim][SCN]	331717–63-6	>0.98	<2000[a]/212[b]	≤2 wt%[a]
1-ethyl-3-methylimidazolium tricyanomethanide	[Emim][$C(CN)_3$]	666823–18-3	>0.98	<1000[a]/146[b]	≤0.5 wt%[a]

[a] Declared by the supplier (IoLiTec, Germany).
[b] Water content measured after drying.

2.5. Viscosity measurement

The viscosity of INFs at 25 °C was determined using rotary viscometer LV DV-II+Pro (Brookfield Engineering, USA) with spindles DIN-86 and DIN-87. The constant temperature of samples during the measurements was provided by Open Bath Circulator ED-5 (Julabo GmbH, Germany) with ethylene glycol. The temperature was controlled via a resistance sensor (RTD) with an uncertainty of ±1 °C and a resolution of 0.1 °C. Each sample was stabilized at the given temperature for a minimum of 30 min until thermal equilibrium was reached. The viscosity curves were determined in shear rate range from 25.8 s^{-1} to 258 s^{-1}. The uncertainty of rheological measurements was estimated at ±3.9% and ±5.4% for DIN-86 and DIN-87, respectively.

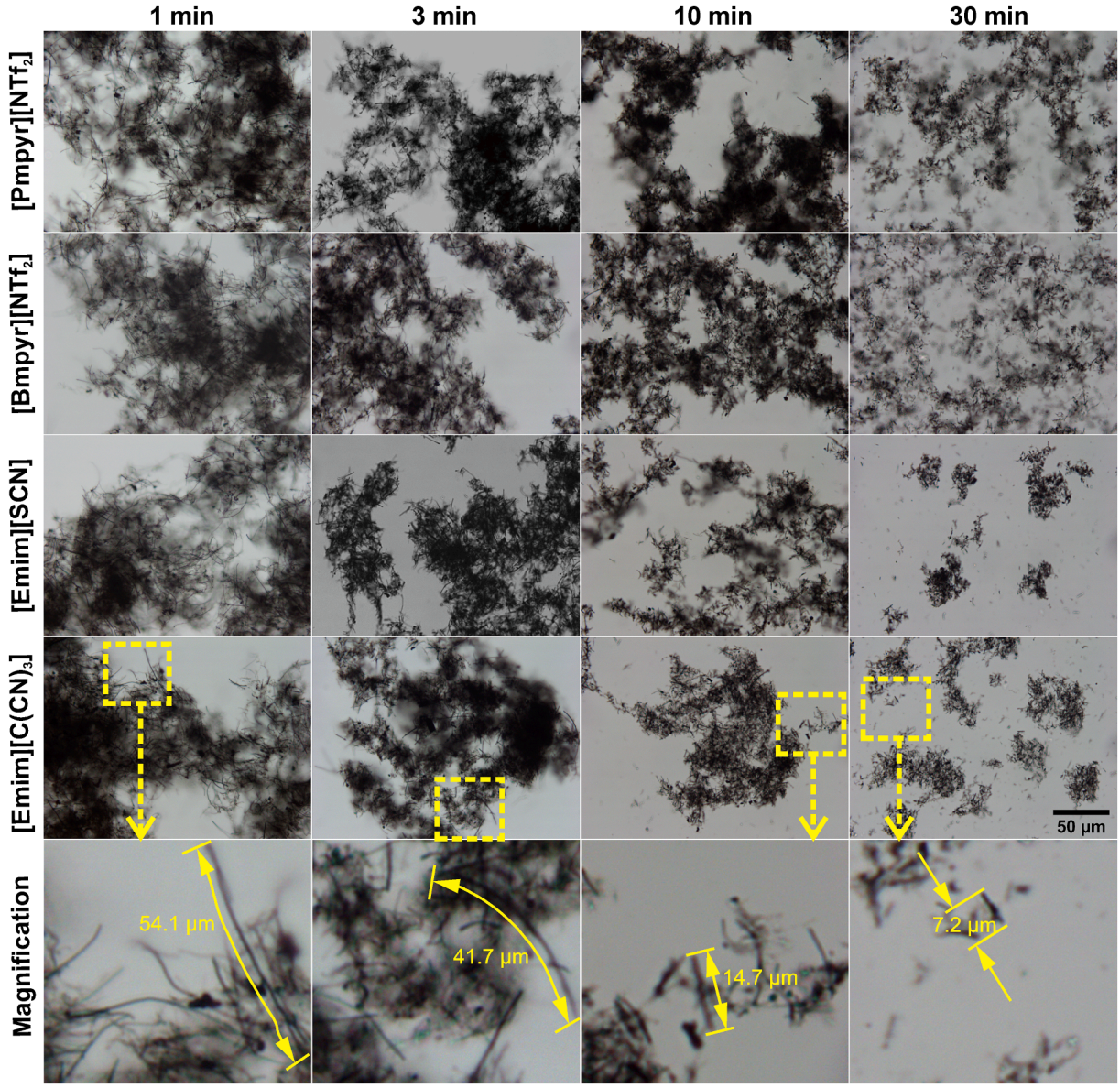

Fig. 2. Optical micrographs of INFs containing 0.2 wt% 'in-house 16h' MWCNTs dispersed in [Pmpyr][NTf_2], [Bmpyr][NTf_2], [Emim][SCN], and [Emim][$C(CN)_3$] (rows) depending on the ultrasonication time (columns). The 50 µm scale bar is common to all images except the last row where the zoomed image areas and exemplary measurements of MWCNT bundle lengths for [Emim][$C(CN)_3$]-based INFs are shown.

3. Results and discussion

3.1. Microstructure of INFs

First, the effect of ultrasonication time on the microstructure of 0.2 wt% 'in-house 16h' MWCNTs dispersed in [Pmpyr][NTf_2], [Bmpyr][NTf_2], [Emim][SCN], and [Emim][$C(CN)_3$] was analyzed (Fig. 2). As can be seen, there are long cylindrical bundles of nanotubes that are entangled and form large tightly-interconnected agglomerates in ILs. Along with the extension of the sonication time, a significant deagglomeration is visible, which leads directly to a shortening of the interconnected nanotube 3D-networks. Loose MWCNT clusters occur more frequently in the case of INFs with [Emim][SCN] and [Emim][$C(CN)_3$], which may indicate their low stability and a tendency to sedimentation due to local changes in density.

With the high-resolution optical micrographs as well as advanced ImageJ® tools for image enhancement (brightness/contrast), zooming (up to 300%), and manual length measurement (straight/segmented lines), the 150 values of MWCNT bundle lengths were determined for each INF. Exemplary measurements for nanodispersions with [Emim][$C(CN)_3$] are shown in the last two rows of Fig. 2. From the microscopic analysis of all samples, it can be concluded that depending on sonication time of 1, 3, 10, and 30 min, the length of nanotube bundles changes in wide ranges of 8.4–49.9, 2.9–32.0, 2.5–23.9, and 2.0–16.2 μm for [Pmpyr][NTf_2]-based INF; 7.9–53.5, 2.5–32.1, 2.3–23.5, and 1.8–12.8 μm for [Bmpyr][NTf_2]-based INF; 5.9–119.1, 6.1–55.1, 3.4–29.8, and 1.6–19.2 μm for [Emim][SCN]-based INF; as well as 7.6–78.3, 5.1–59.5, 4.1–26.4, and 2.3–18.8 μm for [Emim][$C(CN)_3$]-based INF (see detailed histograms in Figs. 3 and 4). Calculated polydispersity index varies between 0.35 and 0.40 for INFs containing [Pmpyr][NTf_2] and [Bmpyr][NTf_2], between 0.37 and 0.50 for INFs with [Emim][$C(CN)_3$], and between 0.44 and 0.59 for INFs based on [Emim][SCN], depending on duration of ultrasound treatment. The results indicate that the microstructure of INFs is non-homogeneous, especially in the case of nanodispersions containing [Emim][SCN] and [Emim][$C(CN)_3$]. However, the bundle size distribution is significantly narrowed when applying longer ultrasound treatment. For 1 min sonication, the average length of the MWCNT bundles is 19.6, 20.6, 23.8, and 27.1 μm for INFs with [Bmpyr][NTf_2], [Pmpyr][NTf_2], [Emim][SCN], and [Emim][$C(CN)_3$], respectively, and decreases by approx. 70% (i.e., up to 5.8, 7.0, 7.2, and 8.1 μm) when extending the process to 30 min (Fig. 5). A similar relationship was observed by Yu et al. [39] (SWCNTs/sodium deoxycholate/water, sonication 30–120 min). In our case, the individualization/fragmentation of MWCNT bundles is noticeably stronger for INFs with [Pmpyr][NTf_2] and [Bmpyr][NTf_2]. The most significant changes in bundle length are observed at the beginning of the ultrasound treatment (within the first 3 min). Extension of the sonication time promotes their homogenization and reduction of variance/polydispersity index (Figs. 3 and 4). These statistical results suggest that sonication provides an effective way to precisely control the length distribution of MWCNT bundles in INFs. It is worth mentioning that in the case of other INFs with nanoparticles of a different morphology like TiO_2, researchers observed only a slight decrease of agglomerate sizes with increasing sonication time (up to 4 h), which did not lead to an improvement in dispersion quality [32,33]

3.2. Thermal conductivity of INFs

Another examined relationship was the effect of sonication time on the thermal conductivity of INFs. As can be seen in Fig. 6, both pure pyrrolidinium-based ILs are characterized by a similar thermal conductivity of 0.120 $W{\cdot}m^{-1}{\cdot}K^{-1}$, regardless of the length of alkyl side chain on their cations. Similarly, both pristine imidazolium-based ILs have the same thermal conductivity of 0.180 $W{\cdot}m^{-1}{\cdot}K^{-1}$, regardless of the size of ions and the number of −CN groups. The addition of 0.2 wt% 'in-house 16h' MWCNTs causes an increase in thermal conductivity of INFs sonicated for 1 min by 6.9%, 7.2%, 11%, and 12% compared to pristine ILs [Emim][$C(CN)_3$], [Emim][SCN], [Bmpyr][NTf_2], and

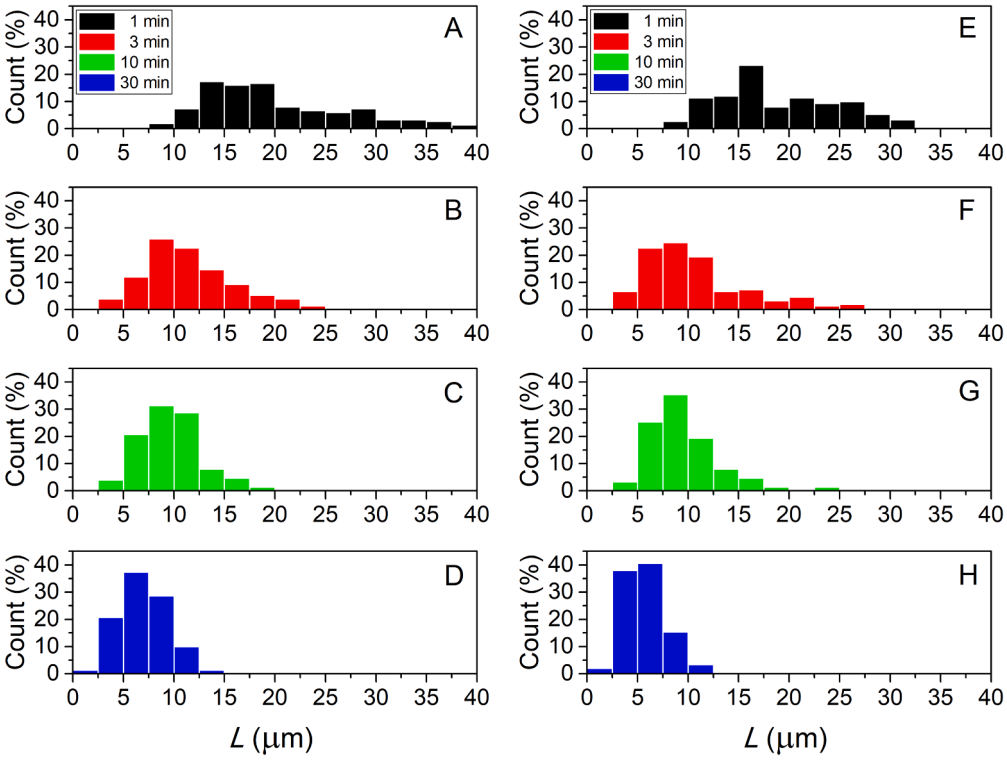

Fig. 3. Histograms of nanotube bundle lengths (*L*) in INFs containing 0.2 wt% 'in-house 16h' MWCNTs dispersed in: (A–D) [Pmpyr][NTf_2] and (E–H) [Bmpyr][NTf_2], depending on the sonication time.

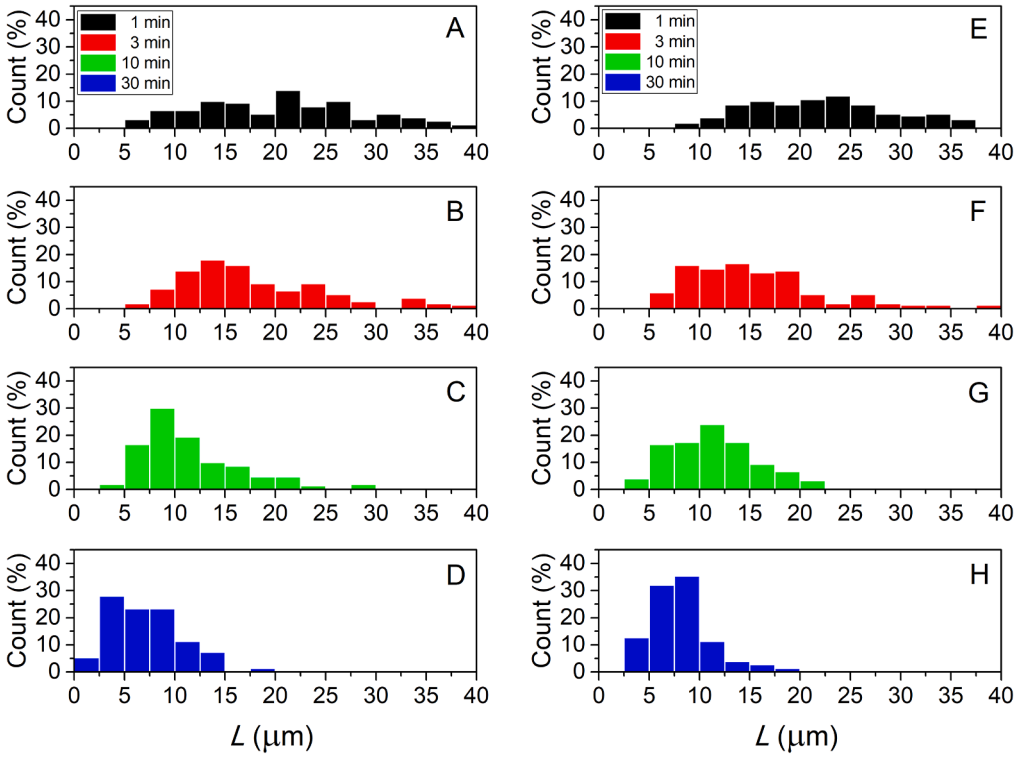

Fig. 4. Histograms of nanotube bundle lengths (L) in INFs containing 0.2 wt% 'in-house 16h' MWCNTs dispersed in: (A–D) [Emim][SCN] and (E–H) [Emim][C(CN)$_3$], depending on the sonication time.

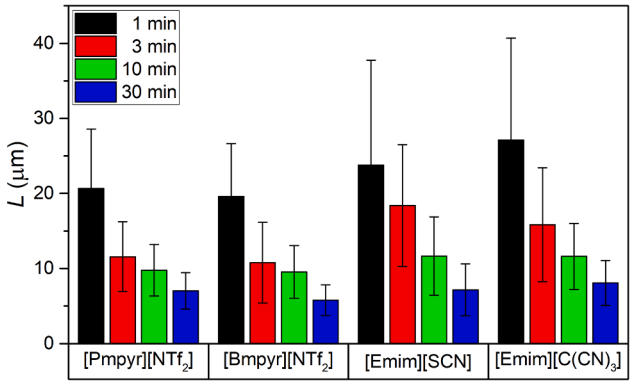

Fig. 5. Average nanotube bundle lengths (L) in INFs containing 0.2 wt% 'in-house 16h' MWCNTs dispersed in [Pmpyr][NTf$_2$], [Bmpyr][NTf$_2$], [Emim][SCN], and [Emim][C(CN)$_3$], depending on the sonication time.

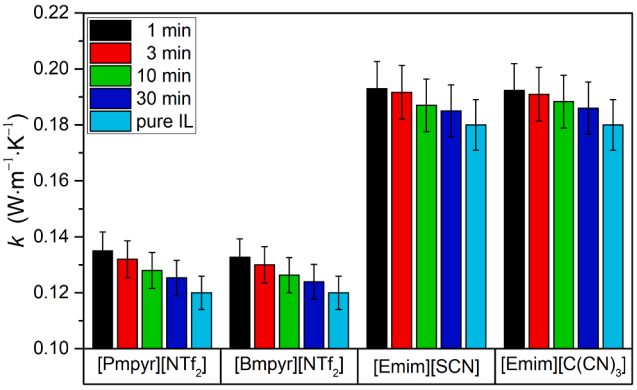

Fig. 6. Thermal conductivity (k) of INFs containing 0.2 wt% 'in-house 16h' MWCNTs dispersed in [Pmpyr][NTf$_2$], [Bmpyr][NTf$_2$], [Emim][SCN], and [Emim][C(CN)$_3$] at 25 °C, depending on the sonication time.

[Pmpyr][NTf$_2$], respectively. However, the thermal conductivity of all analyzed INFs decreases with prolonged ultrasound treatment, showing almost linear decay on a logarithmic time scale. Extension of the process from 1 min to 30 min reduces the thermal conductivity by 3.3%, 4.1%, 6.5, and 7.2% for INFs based on [Emim][C(CN)$_3$], [Emim][SCN], [Bmpyr][NTf$_2$], and [Pmpyr][NTf$_2$], respectively. The achieved results are different from those typically observed in conventional NFs. For instance, Amrollahi et al. [37] (SWCNTs/ethylene glycol, sonication 1–24 h) and Gangadevi et al. [44] (CuO/water, Al_2O_3/water, sonication 1–4 h) noted a continuous enhancement in thermal conductivity of NFs with sonication time, while Zheng et al. [45] (Fe_3O_4/liquid paraffin, sonication 2–4 h) and Asadi et al. [38] (MWCNTs/water, sonication 10–80 min) reported that with increasing sonication time first the thermal conductivity was gradually enhanced, then reached its maximum (at 3 h and 1 h, respectively), and finally began to decline. Nevertheless, some other researchers like Sadeghi et al. [46] (Al_2O_3/water, sonication 0–3 h) and Mahbubul et al. [47] (Al_2O_3/water, sonication 0–5 h) also pointed out the possibility of a decrease in the thermal conductivity of NFs at low sonication times (<0.5 h or 1 h, respectively). In our case, the decline in thermal conductivity of INFs can be explained by the size reduction of MWCNT agglomerates in ILs, as illustrated in the microstructure analysis section. Smaller clusters occupy less space, thus, the effective volume fraction of MWCNTs is lower [37].

3.3. Viscosity of INFs

The last stage of the research included the analysis of the effect of ultrasound exposure time on the rheological properties of INFs. Fig. 7 shows the so-called viscosity curves. Clearly, it can be seen that the viscosity of INFs strongly depends on the viscosity of base ILs. When

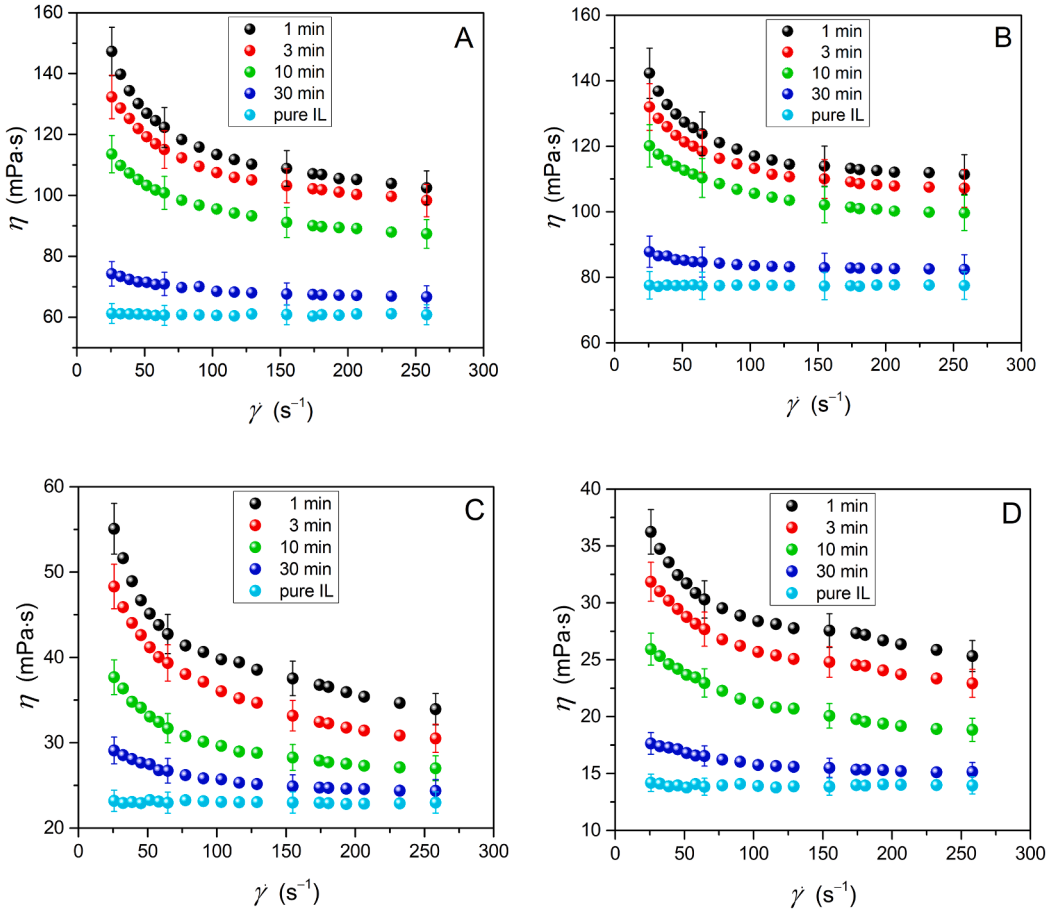

Fig. 7. Viscosity (η) as a function of shear rate ($\dot{\gamma}$) for INFs containing 0.2 wt% 'in-house 16h' MWCNTs dispersed in: (A) [Pmpyr][NTf_2], (B) [Bmpyr][NTf_2], (C) [Emim][SCN], and (D) [Emim][$C(CN)_3$] at 25 °C, depending on the sonication time.

using [Pmpyr][NTf_2] and [Bmpyr][NTf_2] (Fig. 7A,B), the viscosity is found to be more than three times higher compared to INFs consisting of [Emim][SCN] and [Emim][$C(CN)_3$] (Fig. 7C,D). For instance, at shear rate of 32.3 s^{-1}, the addition of 0.2 wt% 'in-house 16h' MWCNTs significantly increases the viscosity of INFs sonicated for 1 min by 129%, 77%, 125%, and 146% compared to pristine ILs [Pmpyr][NTf_2], [Bmpyr][NTf_2], [Emim][SCN], and [Emim][$C(CN)_3$], respectively. All analyzed ILs are Newtonian, while the addition of 'in-house 16h' MWCNTs causes the appearance of non-Newtonian shear-thinning (pseudoplastic) properties. Such rheological behavior of INFs may arise from the reversible disruption of intermolecular interactions, as well as the orientation of MWCNTs in the flow direction, which reduces the flow resistance [48–50]. Both the viscosity and non-Newtonian properties of INFs decline with increasing sonication time. For example, extension of the ultrasound treatment from 1 min to 30 min reduces the viscosity at shear rate of 32.3 s^{-1} by 48%, 37%, 45%, and 50% for INFs based on [Pmpyr][NTf_2], [Bmpyr][NTf_2], [Emim][SCN], and [Emim][$C(CN)_3$], respectively. Similar observations were reported by Vikash and Kumar [51], who studied ultrasound-assisted deagglomeration of silica nanoparticles in water and glycerol. In fact, for a sonication time of 30 min, our analyzed INFs show small deviations from Newtonian behavior. This is the result of a significant reduction in the size and homogenization of carbon agglomerates in ILs [49].

4. Conclusions

Our work is the first to analyze the effect of ultrasonication time on the microstructure, thermal and rheological properties of INFs. A detailed analysis of the results shows that the nanodispersions contain cylindrical bundles of 'in-house 16h' MWCNTs which form large tightly-interconnected agglomerates in ILs. INFs are non-Newtonian shear-thinning media that are characterized by enhanced thermal conductivity and viscosity. The increase in sonication time during sample preparation causes deagglomeration, homogenization, and shortening of MWCNT bundles, as a result of which thermal conductivity, viscosity, and non-Newtonian properties are significantly reduced, approaching the values achieved by pure ILs, e.g., an extension of ultrasound treatment from 1 to 30 min decreases the thermal conductivity of [Bmpyr][NTf_2]-based INF from 0.135 to 0.125 $W{\cdot}m^{-1}{\cdot}K^{-1}$ (i.e., by 7.2%), while thermal conductivity of pristine [Bmpyr][NTf_2] is equal to 0.120 $W{\cdot}m^{-1}{\cdot}K^{-1}$. The thermophysical properties of INFs strongly depend on the type of base ionic liquid. INFs containing imidazolium-based ILs, [Emim][SCN] and [Emim][$C(CN)_3$], have higher average length and polydispersity index of nanotube bundle lengths, as well as lower viscosity, higher thermal conductivity, and much lower stability than nanodispersions based on pyrrolidinium-based ILs, [Pmpyr][NTf_2] and [Bmpyr][NTf_2].

Our work shows that the thermophysical properties of INFs strongly depend on the operating conditions of ultrasound treatment; hence, there is a need for further studies at different ultrasonication parameters, such as pulse amplitude and frequency, energy input, or bath-type treatment. Additionally, a comprehensive understanding of mechanisms governing the ultrasonication-assisted nanotube cleavage in various ILs and the accompanying physicochemistry at the CNT-IL interface must be studied in the forthcoming future as this would enable a range of applications with the heat transfer fluidics as the most pressing one.

CRediT authorship contribution statement

Bertrand Jóźwiak: Conceptualization, Methodology, Validation, Formal analysis, Investigation, Data curation, Visualization, Writing - review & editing, Writing - original draft. **Heather F. Greer:** Investigation, Methodology, Resources. **Grzegorz Dzido:** Investigation, Data curation, Resources. **Anna Kolanowska:** Investigation, Resources. **Rafał Jędrysiak:** Investigation, Resources. **Justyna Dziadosz:** Investigation, Resources. **Marzena Dzida:** Conceptualization, Methodology, Validation, Investigation, Resources, Writing - original draft, Writing - review & editing, Supervision, Project administration, Funding acquisition. **Sławomir Boncel:** Conceptualization, Methodology, Validation, Investigation, Resources, Writing - original draft, Visualization, Writing - review & editing, Supervision, Project administration, Funding acquisition.

Declaration of Competing Interest

The authors declare that they have no known competing financial interests or personal relationships that could have appeared to influence the work reported in this paper.

Acknowledgments

This work was financially supported by the National Science Centre (Poland) Grant No. 2017/27/B/ST4/02748. HFG thanks the EPSRC Underpinning Multi-User Equipment Call (EP/P030467/1) for funding the TEM.

References

[1] S.I. Vieira, M.J.V. Lourenço, J.M. Alves, C.A.N. de Castro, Using ionic liquids and MWCNT's (Ionanofluids) in pigment development, J. Nanofluids 1 (2) (2012) 148–154, https://doi.org/10.1166/jon.2012.1017.
[2] A.A. Minea, S.M.S. Murshed, A review on development of ionic liquid based nanofluids and their heat transfer behavior, Renewable Sustainabe Energy Rev 91 (2018) 584–599, https://doi.org/10.1016/j.rser.2018.04.021.
[3] K. Oster, C. Hardacre, J. Jacquemin, A.P.C. Ribeiro, A. Elsinawi, Understanding the heat capacity enhancement in ionic liquid-based nanofluids (ionanofluids), J. Mol. Liq. 253 (2018) 326–339, https://doi.org/10.1016/j.molliq.2018.01.025.
[4] N. Saurín, T. Espinosa, J. Sanes, F.-J. Carrión, M.-D. Bermúdez, Ionic nanofluids in tribology, Lubricants 3 (2015) 650–663, https://doi.org/10.3390/lubricants3040650.
[5] B. Jóźwiak, S. Boncel, Rheology of ionanofluids – a review, J. Mol. Liq. 302 (2020) 112568, https://doi.org/10.1016/j.molliq.2020.112568.
[6] C.A. Nieto de Castro, X. Paredes, S. Vieira, S. Murshed, M.J. Lourenço, F. Santos, IoNanofluids: innovative agents for sustainable development, in: Nanotechnol. Energy Sustain, Wiley, New York, USA, 2017, pp. 911–936, https://doi.org/10.1002/9783527696109.ch37.
[7] R. Rao, C.L. Pint, A.E. Islam, R.S. Weatherup, S. Hofmann, E.R. Meshot, F. Wu, C. Zhou, N. Dee, P.B. Amama, J. Carpena-Nuñez, W. Shi, D.L. Plata, E.S. Penev, B. I. Yakobson, P.B. Balbuena, C. Bichara, D.N. Futaba, S. Noda, H. Shin, K.S. Kim, B. Simard, F. Mirri, M. Pasquali, F. Fornasiero, E.I. Kauppinen, M. Arnold, B. A. Cola, P. Nikolaev, S. Arepalli, H.-M. Cheng, D.N. Zakharov, E.A. Stach, J. Zhang, F. Wei, M. Terrones, D.B. Geohegan, B. Maruyama, S. Maruyama, Y. Li, W. W. Adams, A.J. Hart, Carbon nanotubes and related nanomaterials: critical advances and challenges for synthesis toward mainstream commercial applications, ACS Nano. 12 (12) (2018) 11756–11784, https://doi.org/10.1021/acsnano.8b06511.
[8] B. Jóźwiak, G. Dzido, A. Kolanowska, R.G. Jędrysiak, E. Zorębski, H.F. Greer, M. Dzida, S. Boncel, From lab and up: superior and economic heat transfer performance of ionanofluids containing long carbon nanotubes and 1-ethyl-3-methylimidazolium thiocyanate, Int. J. Heat Mass Transfer 172 (2021) 121161, https://doi.org/10.1016/j.ijheatmasstransfer.2021.121161.
[9] A. Afzal, I. Nawfal, I.M. Mahbubul, S.S. Kumbar, An overview on the effect of ultrasonication duration on different properties of nanofluids, J. Therm. Anal. Calorim. 135 (1) (2019) 393–418, https://doi.org/10.1007/s10973-018-7144-8.
[10] B. Bakthavatchalam, K. Habib, R. Saidur, B.B. Saha, K. Irshad, Comprehensive study on nanofluid and ionanofluid for heat transfer enhancement: a review on current and future perspective, J. Mol. Liq. 305 (2020) 112787, https://doi.org/10.1016/j.molliq.2020.112787.
[11] W. Yu, H. Xie, A review on nanofluids: preparation, stability mechanisms, and applications, J. Nanomater. 2012 (2012) 1–17, https://doi.org/10.1155/2012/435873.
[12] Z. Baig, O. Mamat, M. Mustapha, A. Mumtaz, K.S. Munir, M. Sarfraz, Investigation of tip sonication effects on structural quality of graphene nanoplatelets (GNPs) for superior solvent dispersion, Ultrason. Sonochem. 45 (2018) 133–149, https://doi.org/10.1016/j.ultsonch.2018.03.007.
[13] A. Sesis, M. Hodnett, G. Memoli, A.J. Wain, I. Jurewicz, A.B. Dalton, J.D. Carey, G. Hinds, Influence of acoustic cavitation on the controlled ultrasonic dispersion of carbon nanotubes, J. Phys. Chem. B. 117 (48) (2013) 15141–15150, https://doi.org/10.1021/jp410041y.
[14] D.V. Kosynkin, A.L. Higginbotham, A. Sinitskii, J.R. Lomeda, A. Dimiev, B.K. Price, J.M. Tour, Longitudinal unzipping of carbon nanotubes to form graphene nanoribbons, Nature 458 (7240) (2009) 872–876, https://doi.org/10.1038/nature07872.
[15] A.M. Dimiev, A. Khannanov, I. Vakhitov, A. Kiiamov, K. Shukhina, J.M. Tour, Revisiting the mechanism of oxidative unzipping of multiwall carbon nanotubes to graphene nanoribbons, ACS Nano. 12 (4) (2018) 3985–3993, https://doi.org/10.1021/acsnano.8b01617.
[16] L. Jiao, X. Wang, G. Diankov, H. Wang, H. Dai, Facile synthesis of high-quality graphene nanoribbons, Nat. Nanotechnol. 5 (5) (2010) 321–325, https://doi.org/10.1038/nnano.2010.54.
[17] Y.-S. Li, J.-L. Liao, S.-Y. Wang, W.-H. Chiang, Intercalation-assisted longitudinal unzipping of carbon nanotubes for green and scalable synthesis of graphene nanoribbons, Sci. Rep. 6 (2016) 22755, https://doi.org/10.1038/srep22755.
[18] K.L. Lu, R.M. Lago, Y.K. Chen, M.L.H. Green, P.J.F. Harris, S.C. Tsang, Mechanical damage of carbon nanotubes by ultrasound, Carbon 34 (6) (1996) 814–816, https://doi.org/10.1016/0008-6223(96)89470-X.
[19] H.B. Chew, M.-W. Moon, K.R. Lee, K.-S. Kim, Compressive dynamic scission of carbon nanotubes under sonication: fracture by atomic ejection, Proc. R. Soc. Math. Phys. Eng. Sci. 467 (2129) (2011) 1270–1289, https://doi.org/10.1098/rspa.2010.0495.
[20] K. Oster, C. Hardacre, J. Jacquemin, A.P.C. Ribeiro, A. Elsinawi, Ionic liquid-based nanofluids (ionanofluids) for thermal applications: an experimental thermophysical characterization, Pure Appl. Chem. 91 (2019) 1309–1340, https://doi.org/10.1515/pac-2018-1114.
[21] F.-F. Zhang, F.-F. Zheng, X.-H. Wu, Y.-L. Yin, G. Chen, Variations of thermophysical properties and heat transfer performance of nanoparticle-enhanced ionic liquids, R. Soc. Open Sci. 6 (4) (2019) 182040, https://doi.org/10.1098/rsos.182040.
[22] B. Wang, X. Wang, W. Lou, J. Hao, Rheological and tribological properties of ionic liquid-based nanofluids containing functionalized multi-walled carbon nanotubes, J. Phys. Chem. C. 114 (19) (2010) 8749–8754, https://doi.org/10.1021/jp1005346.
[23] W. Chen, C. Zou, X. Li, An investigation into the thermophysical and optical properties of SiC/ionic liquid nanofluid for direct absorption solar collector, Sol. Energy Mater. Sol. Cells 163 (2017) 157–163, https://doi.org/10.1016/j.solmat.2017.01.029.
[24] F. Wang, L. Han, Z. Zhang, X. Fang, J. Shi, W. Ma, Surfactant-free ionic liquid-based nanofluids with remarkable thermal conductivity enhancement at very low loading of graphene, Nanoscale Res. Lett. 7 (1) (2012) 314, https://doi.org/10.1186/1556-276X-7-314.
[25] E.I. Cherecheş, J.I. Prado, M. Cherecheş, A.A. Minea, L. Lugo, Experimental study on thermophysical properties of alumina nanoparticle enhanced ionic liquids, J. Mol. Liq. 291 (2019) 111332, https://doi.org/10.1016/j.molliq.2019.111332.
[26] A. Hosseinghorbani, M. Mozaffarian, G. Pazuki, Application of graphene oxide IoNanofluid as a superior heat transfer fluid in concentrated solar power plants, Int. Commun. Heat Mass Transfer 111 (2020) 104450, https://doi.org/10.1016/j.icheatmasstransfer.2019.104450.
[27] E.I. Cherecheş, D. Bejan, C. Ibanescu, M. Danu, A.A. Minea, Ionanofluids with [C2mim][CH3SO3] ionic liquid and alumina nanoparticles: an experimental study on viscosity, specific heat and electrical conductivity, Chem. Eng. Sci. 229 (2021) 116140, https://doi.org/10.1016/j.ces.2020.116140.
[28] S. Jorjani, M. Mozaffarian, G. Pazuki, A novel Nanodiamond based IoNanofluid: experimental and mathematical study of thermal properties, J. Mol. Liq. 271 (2018) 211–219, https://doi.org/10.1016/j.molliq.2018.08.116.
[29] C. Hermida-Merino, A.B. Pereiro, J.M.M. Araújo, C. Gracia-Fernández, J.P. Vallejo, L. Lugo, M.M. Piñeiro, Graphene IoNanofluids, thermal and structural characterization, Nanomaterials 9 (2019) 1549, https://doi.org/10.3390/nano9111549.
[30] B. Bakthavatchalam, K. Habib, R. Saidur, N. Aslfattahi, S.M. Yahya, A. Rashedi, T. Khanam, Optimization of thermophysical and rheological properties of mxene ionanofluids for hybrid solar photovoltaic/thermal systems, Nanomaterials 11 (2021) 320, https://doi.org/10.3390/nano11020320.
[31] C.A. Nieto de Castro, A.P.d.C. Ribeiro, A.O. Figueiras, E. Langa, S.I.C. Vieira, M.J. V. Lourenço, Â.F.S.D. Santos, F.J. Vieira dos Santos, I.M.S. Lampreia, P. Goodrich, C. Hardacre, Thermophysical Properties of 1-Butyl-3-methylimidazolium tris (pentafluoroethyl)trifluorophosphate, [C4mim][(C2F5)3PF3], and of Its IoNanofluid with multi-walled carbon nanotubes, J. Chem. Eng. Data. 66 (4) (2021) 1717–1729, https://doi.org/10.1021/acs.jced.0c01017.
[32] A. Wittmar, M. Ulbricht, Dispersions of Various Titania Nanoparticles in Two Different Ionic Liquids, Ind. Eng. Chem. Res. 51 (25) (2012) 8425–8433, https://doi.org/10.1021/ie203010x.
[33] A. Wittmar, M. Gajda, D. Gautam, U. Dörfler, M. Winterer, M. Ulbricht, Influence of the cation alkyl chain length of imidazolium-based room temperature ionic liquids on the dispersibility of TiO2 nanopowders, J. Nanoparticle Res. 15 (2013) 1463, https://doi.org/10.1007/s11051-013-1463-2.
[34] J.M.P. França, M.J.V. Lourenço, S.M.S. Murshed, A.A.H. Pádua, C.A. Nieto de Castro, Thermal conductivity of ionic liquids and ionanofluids and their feasibility as heat transfer fluids, Ind. Eng. Chem. Res. 57 (18) (2018) 6516–6529, https://doi.org/10.1021/acs.iecr.7b04770.

[35] J.J. Wang, R.T. Zheng, J.W. Gao, G. Chen, Heat conduction mechanisms in nanofluids and suspensions, NANO Today 7 (2) (2012) 124–136, https://doi.org/10.1016/j.nantod.2012.02.007.
[36] R. Zheng, J. Gao, J. Wang, S.-P. Feng, H. Ohtani, J. Wang, G. Chen, Thermal percolation in stable graphite suspensions, NANO Lett. 12 (1) (2012) 188–192, https://doi.org/10.1021/nl203276y.
[37] A. Amrollahi, A.A. Hamidi, A.M. Rashidi, The effects of temperature, volume fraction and vibration time on the thermo-physical properties of a carbon nanotube suspension (carbon nanofluid), Nanotechnology 19 (31) (2008) 315701, https://doi.org/10.1088/0957-4484/19/31/315701.
[38] A. Asadi, I.M. Alarifi, V. Ali, H.M. Nguyen, An experimental investigation on the effects of ultrasonication time on stability and thermal conductivity of MWCNT-water nanofluid: Finding the optimum ultrasonication time, Ultrason. Sonochem. 58 (2019) 104639, https://doi.org/10.1016/j.ultsonch.2019.104639.
[39] H. Yu, S. Hermann, S.E. Schulz, T. Gessner, Z. Dong, W.J. Li, Optimizing sonication parameters for dispersion of single-walled carbon nanotubes, Chem. Phys. 408 (2012) 11–16, https://doi.org/10.1016/j.chemphys.2012.08.020.
[40] A. Asadi, F. Pourfattah, I. Miklós Szilágyi, M. Afrand, G. Żyła, H.o. Seon Ahn, S. Wongwises, H. Minh Nguyen, A. Arabkoohsar, O. Mahian, Effect of sonication characteristics on stability, thermophysical properties, and heat transfer of nanofluids: a comprehensive review, Ultrason. Sonochem. 58 (2019) 104701, https://doi.org/10.1016/j.ultsonch.2019.104701.
[41] B. Jóźwiak, G. Dzido, E. Zorębski, A. Kolanowska, R. Jędrysiak, J. Dziadosz, M. Libera, S. Boncel, M. Dzida, Remarkable thermal conductivity enhancement in carbon-based ionanofluids: effect of nanoparticle morphology, ACS Appl. Mater. Interfaces 12 (34) (2020) 38113–38123, https://doi.org/10.1021/acsami.0c09752.
[42] A. Kazakov, J.W. Magee, R.D. Chirico, E. Paulechka, V. Diky, C.D. Muzny, K. Kroenlein, M. Frenkel, NIST Standard Reference Database 147: Ionic Liquids Database – ILThermo v2.0, National Institute of Standards and Technology, Gaithersburg, USA, 2017.
[43] A. Kolanowska, A. Kuziel, Y. Li, S. Jurczyk, S. Boncel, Rieche formylation of carbon nanotubes – one-step and versatile functionalization route, RSC Adv. 7 (81) (2017) 51374–51381, https://doi.org/10.1039/C7RA10525H.
[44] R. Gangadevi, B.K. Vinayagam, S. Senthilraja, Effects of sonication time and temperature on thermal conductivity of CuO/water and Al2O3/water nanofluids with and without surfactant, Mater. Today Proc. 5 (2) (2018) 9004–9011, https://doi.org/10.1016/j.matpr.2017.12.347.
[45] Y. Zheng, A. Shahsavar, M. Afrand, Sonication time efficacy on Fe3O4-liquid paraffin magnetic nanofluid thermal conductivity: an experimental evaluation, Ultrason. Sonochem. 64 (2020) 105004, https://doi.org/10.1016/j.ultsonch.2020.105004.
[46] R. Sadeghi, S.G. Etemad, E. Keshavarzi, M. Haghshenasfard, Investigation of alumina nanofluid stability by UV–vis spectrum, Microfluid. Nanofluidics 18 (5-6) (2015) 1023–1030, https://doi.org/10.1007/s10404-014-1491-y.
[47] I.M. Mahbubul, I.M. Shahrul, S.S. Khaleduzzaman, R. Saidur, M.A. Amalina, A. Turgut, Experimental investigation on effect of ultrasonication duration on colloidal dispersion and thermophysical properties of alumina–water nanofluid, Int. J. Heat Mass Transfer 88 (2015) 73–81, https://doi.org/10.1016/j.ijheatmasstransfer.2015.04.048.
[48] M. Hojjat, S.G. Etemad, R. Bagheri, J. Thibault, Rheological characteristics of non-Newtonian nanofluids: experimental investigation, Int. Commun. Heat Mass Transfer 38 (2) (2011) 144–148, https://doi.org/10.1016/j.icheatmasstransfer.2010.11.019.
[49] A.G.M. Ferreira, P.N. Simões, A.F. Ferreira, M.A. Fonseca, M.S.A. Oliveira, A.S. M. Trino, Transport and thermal properties of quaternary phosphonium ionic liquids and IoNanofluids, J. Chem. Thermodyn. 64 (2013) 80–92, https://doi.org/10.1016/j.jct.2013.04.013.
[50] R. Pamies, C. Espejo, F.J. Carrión, A. Morina, A. Neville, M.D. Bermúdez, Rheological behavior of multiwalled carbon nanotube-imidazolium tosylate ionic liquid dispersions, J. Rheol. 61 (2) (2017) 279–289, https://doi.org/10.1122/1.4975108.
[51] Vikash, V. Kumar, Ultrasonic-assisted de-agglomeration and power draw characterization of silica nanoparticles, Ultrason. Sonochem. 65 (2020) 105061, https://doi.org/10.1016/j.ultsonch.2020.105061.